



Film cooling on a convex surface with zero pressure gradient flow

E. Lutum^a, J. von Wolfersdorf^a, B. Weigand^{b,*}, K. Semmler^c

^aABB Alstom Technology Ltd., Heat Transfer Group, 5405 Baden-Dättwil, Switzerland

^bUniversity of Stuttgart, Institut für Thermodynamik der Luft- und Raumfahrt, Pfaffenwaldring 31, 70569 Stuttgart, Germany

^cABB Alstom Power Ltd., Gas Turbine Development, 5401 Baden, Switzerland

Received 30 June 1999; received in revised form 6 September 1999

Abstract

The adiabatic film cooling effectiveness and heat transfer increase due to film injection was investigated on a convex surface at zero pressure gradient flow. Film cooling results were obtained using thermochromic liquid crystals to measure the local wall temperature distribution. Five different injection configurations, three with cylindrical and two with shaped holes were examined. Coolant injection with cylindrical holes indicates decreased film cooling effectiveness and increased heat transfer at moderate and high blowing rates. Significant higher film cooling effectiveness values and lower heat transfer increase due to film injection were achieved by shaped hole injection compared to cylindrical hole injection. © 2000 Elsevier Science Ltd. All rights reserved.

Keywords: Experimental; Film cooling; Heat transfer

1. Introduction

In modern gas turbine engine designs, there is a desire to increase the inlet hot-gas temperature of the turbine to increase the cycle efficiency. The use of the most efficient cooling technology available is required on one side by this further increased turbine inlet temperature and by the demand of high gas turbine cycle efficiency on the other side. The application of film cooling is strongly required at these high turbine inlet temperatures to achieve allowable metal temperature limits. The reduction in thermal strain due to the reduction of external gas temperature achieved with the

film cooling is another important feature that guarantees the components life requirements. Although, the development of thermal barrier coating made strong improvements during the last years, its use is still limited.

Film cooling has been extensively studied over the past 30 years and a large part of the results is available in the open literature. Most of these studies concentrate on flat plate configurations with film injection through slots or rows of cylindrical holes. Fewer publications are available concerning film cooling on airfoil type flow or general on curved surfaces. However, those film cooling investigations conducted on curved walls indicate that curvature has a significant influence on the film cooling performance. An overview of the related experimental film cooling investigations is given below.

Nicolas and Le Meur [1], Folyan and Whitelaw [2],

* Corresponding author. Tel.: +49-711-685-3590; fax: +49-711-685-2317.

E-mail address: bw@itlr.uni-stuttgart.de (B. Weigand).

Nomenclature

AR	outlet to inlet area ratio of film holes	β	injection angle relative to the free-stream flow, compound angle
C_p	specific heat at constant pressure	δ	boundary layer thickness
D	film hole diameter	δ_1	boundary layer displacement thickness
DR	density ratio between secondary and free-stream fluid, ρ_c/ρ_∞	γ	bend angle position
h	convective heat transfer coefficient	η_{ad}	adiabatic film cooling effectiveness
I	momentum flux ratio, $(\rho_c U_c^2)/(\rho_\infty U_\infty^2)$	φ_1	extension angle in lateral direction
K	acceleration parameter, $(v_\infty/U_\infty^2)(\partial U_\infty/\partial S)$	φ_2	extension angle in stream-wise direction
L	hole length	κ	ratio of gas specific heats
M	blowing rate, $(\rho_c U_c)/(\rho_\infty U_\infty)$	λ	microscale of free-stream turbulence
Ma	Mach number	$\lambda_{Necuron}$	thermal conductivity of Necuron material
\dot{q}	specific heat flux	A	integral length scale of free-stream turbulence
p	static pressure	ρ	fluid density
P	total pressure	Θ	dimensionless wall temperature
P	pitch, lateral spacing of film holes		
Pr	Prandtl number		
P/D	pitch-to-diameter ratio	<i>Subscripts</i>	
R	radius of curved test surface	0	without film cooling
S	stream-wise co-ordinate	aw	adiabatic wall
St	Stanton number	c	coolant fluid
t	static temperature	f	with film cooling
T	total temperature	inj	injection condition
Tu	turbulence intensity	la	lateral averaged
U	mean velocity	r	recovery condition
		w	wall condition
		TLC	thermochromic liquid crystals
		∞	free-stream fluid
<i>Greek symbols</i>			
α	injection angle relative to the test surface		

Mayle et al. [3] and Ito et al. [4] first systematically investigated the curvature influence on film cooling performance. The general trends of these investigations are:

- for low blowing rates, $M = 0.5$, the film cooling performance is increased on convex surfaces and decreased on concave surfaces compared to flat surfaces
- for moderate blowing rates, $M = 1.0$, the film cooling performance is increased on convex surfaces compared to concave and flat surfaces
- for high blowing rates, $M = 2.0$, the film cooling performance is increased on concave surfaces compared to convex and flat surfaces
- the strength of the curvature effects mentioned above are more pronounced on convex surfaces.

There are basically two concepts of film cooling experiments on curved surfaces found in the literature. There are experiments on specific airfoil geometries (vane or blade cascades or turbine test facilities), that are often conducted close to engine boundary conditions. Although, these investigations are very important for the verification of specific designs, they often

do not deliver sufficient information to deduce physical models for other designs with different geometries or boundary conditions. Second category experiments are generic investigations that try to resolve the physical inside of the film cooling process on curved surfaces. The aim of these experimental investigations is to isolate the governing free-stream and secondary flow boundary conditions and to extract the basic influence of the curvature on the film cooling performance.

Ito et al. [4], Rodi et al. [5], Takeishi et al. [6] and Ou and Han [7] conducted airfoil cascade experiments with single row injection. Film cooling experiments with double or multiple row injection were conducted by Lander et al. [8], Goldstein et al. [9] and Takeishi et al. [10]. Takeishi et al. [6,10] presented data correlations of their experimental pressure and suction side results. Additional to their linear cascade data Takeishi et al. [6] reported on film cooling experiments conducted on a single stage turbine rig. Buck and Prakash [11] conducted experiments in a single channel blade passage to simulate free-stream aerodynamics between two adjacent turbine airfoils. Film cooling effectiveness values were

measured for single row injection on suction and pressure sides. Experiments on generic curved wall geometries were investigated by Mayle et al. [3], Ko et al. [12], Kruse [13], Lee et al. [14], Schwarz and Goldstein [15] and Schwarz et al. [16]. The pressure gradient of the free-stream flow was close to zero in all of the above mentioned investigations. Mayle et al. [3] compared flat plate results with data derived from convex and concave walls for slot injection. All other authors conducted film cooling experiments with injection through a single row of cylindrical holes. The investigations from Kruse [13], Schwarz and Goldstein [15] and Schwarz et al. [16] presented results for different ratios of surface curvature to film hole diameter (R/D). A comparison of the curvature results with related flat plate film cooling results is also presented.

Besides the experimental film cooling studies numerous theoretical investigations were performed during the last 25 years that have been compiled by Kercher [17].

Most of the above mentioned studies present film cooling effectiveness data without the corresponding heat transfer information, which is an important input parameter for the thermal design of gas turbine airfoils. Although shaped injection configurations are frequently used in modern cooling designs rarely film cooling results obtained with these shaped holes on curved surfaces are available from the literature. Especially, film shaped hole cooling experiments with accelerated free-stream flow at constant surface curvature is not available from the literature. Therefore, a film cooling test program to study these effects was initiated and is part of the present Brite EuRam Framework IV. The aim of this study is the investigation of film cooling performance on a convex surface. The influence of an accelerated free-stream flow will be presented in a subsequent paper.

Film cooling and heat transfer experiments were performed with a zero pressure gradient free-stream flow. The free-stream turbulence intensity at the injection location was about 5%. The free-stream boundary conditions were kept constant, but the coolant boundary conditions were systematically varied during these film cooling experiments. The blowing rate was varied between $0.5 \leq M \leq 2.0$. The major part of these experiments was conducted with CO_2 as coolant fluid, respectively with a high density ratio. Some measurements with air-injection, respectively with a low density ratio, were also conducted. Film cooling measurements were performed with five different injection configurations, three cylindrical and two shaped injection configurations.

2. Experimental facility

The film cooling test facility with curved and adjustable outer wall was designed to determine the film cooling effectiveness and the heat transfer increase due to film injection along curved surfaces. The investigations reported here were focused on film cooling on a convex surface. Secondary fluid (CO_2 or air) was injected through a single row of cylindrical or shaped holes. The multiple narrow-banded thermochromic liquid crystal technique was used to determine the local wall temperature distributions along the test surface.

Two blowers with a total energy consumption of 720 kW delivered the free-stream air in the open-circuit wind tunnel system. The mass flow capacity of the two blowers in parallel mode was about 10 kg/s at a pressure level of 0.55 bar above atmosphere. The free-stream temperature level was increased up to 80°C by means of an electrical heater (760 kW). The heated free-stream was homogenised in the settling chamber by an assembly of three screens and a honeycomb. A nozzle with a contraction ratio of 3.6:1 was used to guide the free-stream into the rectangular test section with a 200 by 400 mm cross section. The settling chamber and the nozzle were insulated in order to avoid heat losses of the free-stream. A turbulence generator, located at the nozzle exit achieved an increased free-stream turbulence level of about 5% at the injection location. This turbulence grid consisted of nine rectangular bars with 15 mm height. The bars were arranged horizontally and spaced 25 mm apart. A 400 mm straight section provided sufficient length to achieve isotropic turbulence quantities at the entrance of the curved test section. The free-stream followed a 150° -bend within the curved test section. Secondary fluid was injected at a bend angle of $\gamma_{\text{inj}} = 30^\circ$. At the exit of the curved test section a straight section of 700 mm length was inserted to avoid down-stream disturbances of the flow field in the curved test section. The flow left the test section via a connection piece into the silencer and was finally released into the environment from there (see Fig. 1).

The test section shown in Fig. 2 was built up as a sandwich construction, consisting of a bottom and top plate with the inner and outer test section walls in between of them. The 40 mm thick bottom plate provides a solid basis on which the test section walls were built up. The material of the curved inner wall was Necuron, a low conductive polyurethane based material with a thermal conductivity of $\lambda_{\text{Necuron}} = 0.1 \text{ W/(mK)}$. This wall was segmented into three parts where the middle part contains the injection configuration. Different film injection configurations could be installed by interchanging this

middle segment. The upper and lower segments of this wall contain static pressure tapping. The secondary fluid supply system was embedded in the inner test section wall. The secondary fluid was fed into the settling chamber at the bottom and top of this cylindrical settling chamber, which has a diameter of 50 mm. The secondary fluid velocity in the settling chamber was estimated to be not higher than 15 m/s for the highest coolant mass flow (0.1 kg/s), that could be delivered by the CO₂ supply system. The ratio between the area of the settling chamber and the total injection area was 6:1, which assured an even pressure distribution for all injection holes. The outer test section wall consisted of a Poly-

carbonat plate with 5 mm thickness. Polycarbonat is a polyester based material, similar to Plexiglas, with good mechanical and optical properties. The shape of this thin Polycarbonat wall was settled by several flexible fixations at $\gamma = 0^\circ, 30^\circ, 60^\circ, 90^\circ, 120^\circ$ and 150° of the bend and two extra fixations at the test section outlet (see Fig. 2). This flexible outer wall design allowed moderate adjustments to a specific Polycarbonat wall shape and hence moderate adjustments to the flow field in the test section. Furthermore, it allowed the replacement with another Polycarbonat wall, with a different shape, to achieve different free-stream boundary conditions, for example an accelerated free-stream flow. A welded steel construction represented

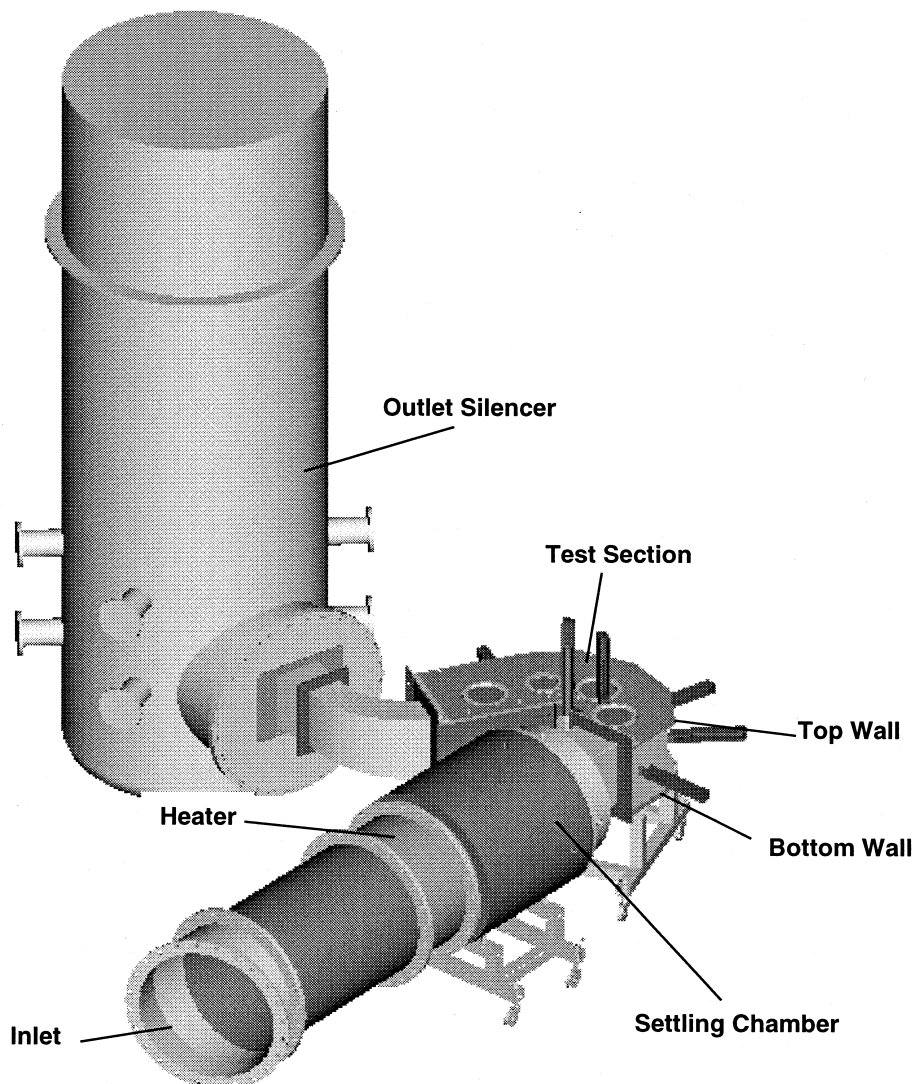


Fig. 1. Curved wall film cooling test facility.

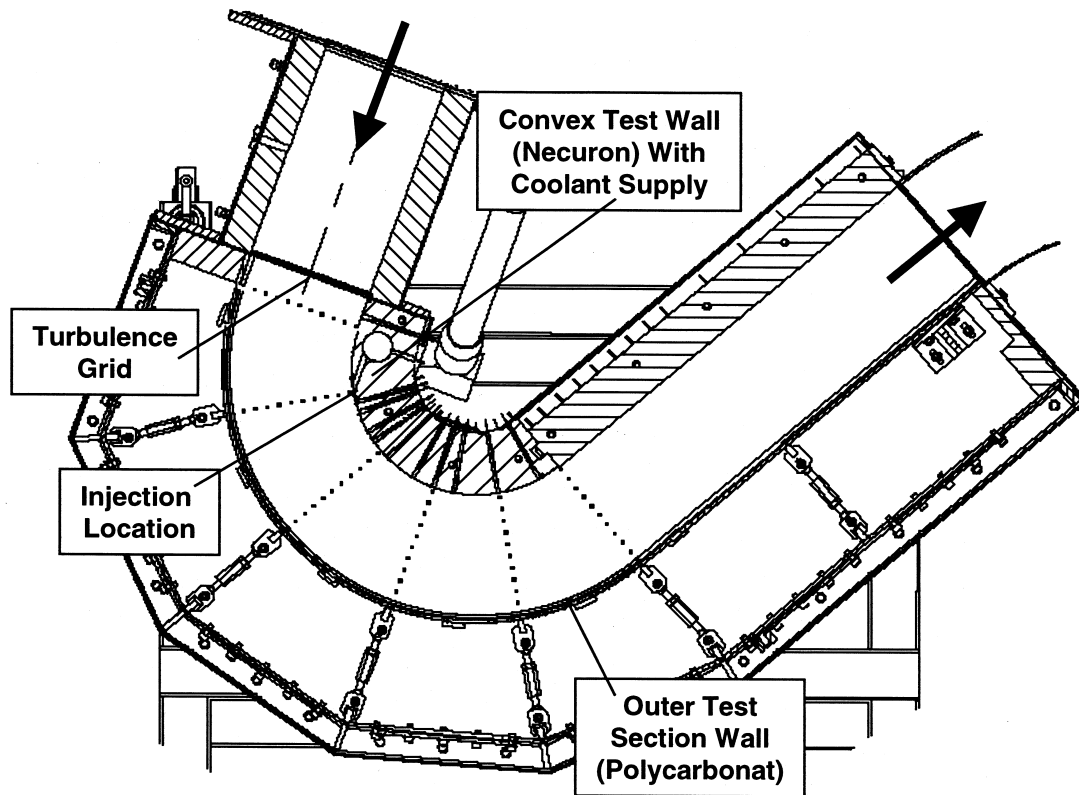


Fig. 2. Convex test section.

the solid outside border of the test section. The above mentioned fixations for the Polycarbonat wall were attached to this steel construction. Seven glass windows in this outer steel frame allowed optical access into the test section.

A total number of five film injection configurations were investigated. Injection configuration CONF 1 (see Fig. 3) consisted of a row of nine cylindrical holes. The injection angle of the film holes was $\alpha = 30^\circ$ relative to the surface. The holes were spaced three hole diameters in lateral direction, $P/D = 3.0$ and had a hole length-to-diameter ratio of $L/D = 7.5$. The second cylindrical injection geometry, injection configuration CONF 2 shown in Fig. 3 had a lateral spacing of $P/D = 6.0$. Injection configuration CONF 3, also shown in Fig. 3, consisted also of a row of five cylindrical holes, that were inclined at $\alpha = 30^\circ$ to the surface and $\beta = 60^\circ$ to the free-stream flow direction (compound angle). The lateral spacing of the holes was again $P/D = 6.0$.

Injection configuration CONF 4 (see Fig. 4) consisted of a row of five shaped holes, inclined at $\alpha = 30^\circ$ to the test surface. The lateral spacing of the holes was

$P/D = 6.0$, related to the throat diameter of the cylindrical entrance section of the shaped film holes. This cylindrical part of the hole channels had a length of 2.5 hole diameter. The remaining length, $L/D = 5.0$, of the hole channels were laterally opened. The outlet to inlet area ratio of $AR = 3.7$ was produced by the fan angle of $\varphi_1 = 12^\circ$. Fig. 4 also shows injection configuration CONF 5 that was similar to injection configuration CONF 4. Additionally to the lateral extension angle φ_1 a laid back angle φ_2 was introduced in this injection configuration. This streamwise widening of the film holes, $\varphi_2 = 15^\circ$, reduced the effective injection angle of the secondary fluid relative to the surface. Injection configuration CONF 5 had also an area ratio of $AR = 3.7$.

3. Measurement technique

The surface temperature data was obtained by use of the narrow-banded thermochromic liquid crystal technique. This measurement technique was used for both types of experiments, adiabatic and heat transfer film cooling measurements. Isothermal temperature

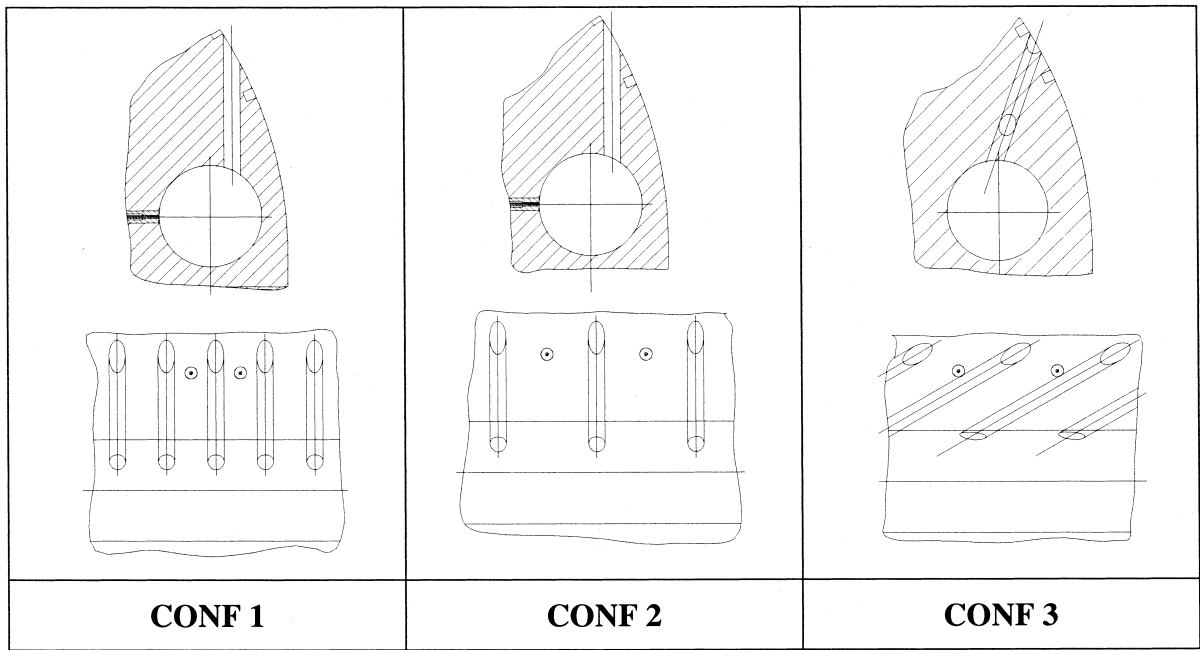


Fig. 3. Film cooling geometries with cylindrical injection holes.

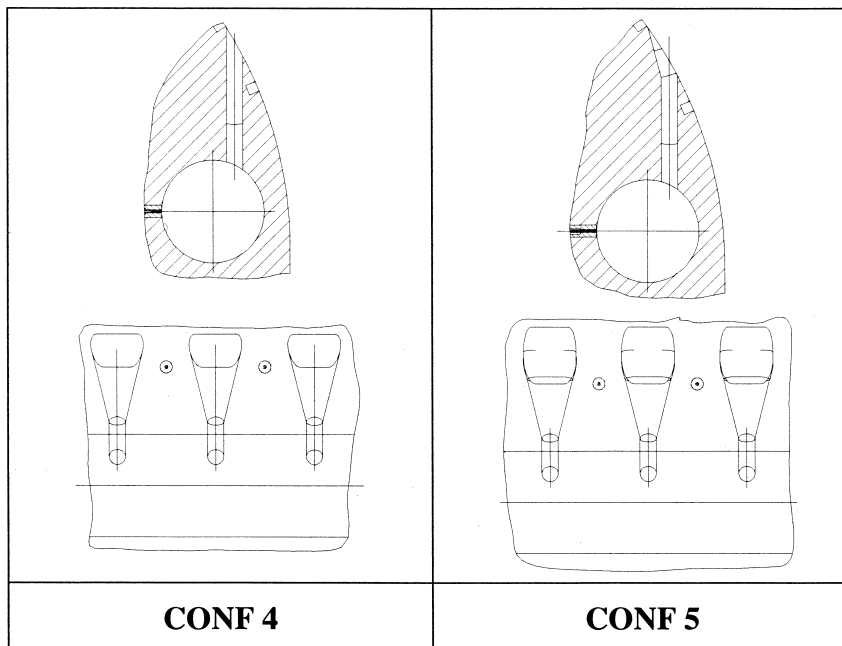


Fig. 4. Film cooling geometry with shaped injection holes.

patterns on the test surface were indicated by narrow-banded thermochromic liquid crystals and were observed by a colour image processing system. All additional experimental data, i.e., temperature, pressure and velocity information of the free-stream and secondary flow was recorded by a separate data acquisition system for later data reduction purposes.

To achieve accurate film cooling data, a special set-up was built to conduct the temperature calibration of the narrow-banded thermochromic liquid crystal indication temperature. The copper plate, used for this calibration, was coated with the same thermochromic liquid crystals as the test surface. Heating at one end of this plate and cooling at the other end achieved a linear temperature distribution. Determination of the indication temperature of the thermochromic liquid crystals on the copper surface was obtained with the same colour image processing system used later for the film cooling measurements. Thermocouples, embedded in the copper surface, were used to measure the reference temperature distribution along the plate length. During the experiments, the thermochromic liquid crystal indications were captured using a CCD-camera in conjunction with image processing techniques. A full picture was built up using several adjacent smaller images. The CCD camera was mounted aside the experimental apparatus to observe the test surface at several streamwise positions. Using multiple images to build up the final picture allows higher resolution and better picture definition. The image data files were colated to create the full picture by using a specially prepared computer program. This allowed the final raw data set to be imported directly into a standard graphics package for further image processing operations for better definition of the isothermal contour lines.

During the adiabatic film cooling experiments the temperature indications of the thermochromic liquid crystals, T_{TLC} , were assumed to be the local adiabatic wall temperatures T_{aw} . With the additional information of the free-stream recovery $T_{r\infty}$ and secondary fluid T_c total temperatures these isothermal contour lines were transformed into adiabatic film cooling effectiveness contours, η_{ad} ,

$$\eta_{ad} = \frac{T_{r\infty} - T_{aw}}{T_{r\infty} - T_c} \tag{1}$$

where the recovery temperature of the free-stream flow was obtained using

$$T_{r,\infty} = T_\infty + (Pr_\infty^{1/3} - 1) \frac{U_\infty^2}{2C_{p\infty}} \tag{2}$$

In case of constant heat flux experiments with and without film cooling the thermochromic liquid crystal

temperature, T_{TLC} , indicated the local wall temperatures T_w . For the measurements without film cooling the film cooling holes were covered with a thin aluminium tape to avoid additional sources of flow disturbances, that would increase heat transfer. The heat transfer coefficient in the absence of film cooling was calculated by

$$h_0 = \frac{\dot{q}_0}{T_{r\infty} - T_{rw}} \tag{3}$$

where \dot{q}_0 is the constant heat flux without film cooling, created by electrical current send through the steel foil. Assuming that the electrical energy introduced into the steel foil was totally transformed into heat, due to foil resistance, \dot{q}_0 was determined from

$$\dot{q}_0 = R_{sp} I^2 \tag{4}$$

where R_{sp} is the specific foil resistance per unit area and I is the electrical current introduced into the foil. For the experiments with film cooling the heat transfer coefficients were defined by

$$h_f = \frac{\dot{q}_f}{T_{aw} - T_{rw}} \tag{5}$$

where \dot{q}_f is the constant heat flux with film cooling and

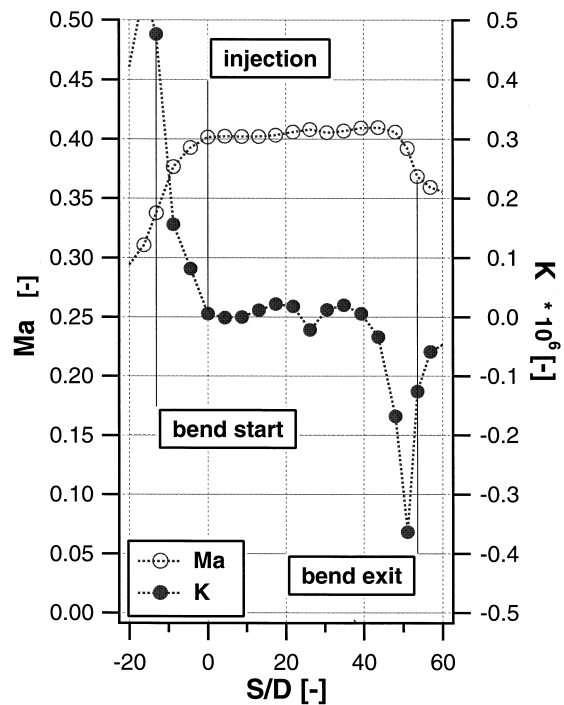


Fig. 5. Distributions of the free-stream Mach number and acceleration parameter versus streamwise distance.

T_{aw} is the adiabatic wall temperature. For simplicity, the heat transfer experiments were conducted at iso-energetic conditions ($T_c = T_\infty$). The heat losses into the low conductive wall have been estimated by heat conduction analysis. The temperature error due to this heat loss was less than 0.1°C.

For the calculation of the lateral averaged film cooling effectiveness values and the lateral averaged heat transfer coefficients, a special interpolation routine was created. Lutum and Johnson [18] gave a detailed description of the measurement procedure, data reduction method and data uncertainty. Local film cooling effectiveness values were determined by this uncertainty analysis to be not higher than 0.008. Typical interpolation accuracy was within 2.5% of the local effectiveness value. The integration error based on experimental and interpolation uncertainty was about 1–3% of the streamwise local lateral averaged film cooling effectiveness with the higher uncertainty related to lower effectiveness values.

4. Results and discussion

Aerodynamic measurements without secondary fluid injection were conducted to characterise the free-

stream flow in the test section. Hot-wire traverses were conducted at several locations within the convex test section. The boundary layer thickness, the displacement thickness and the free-stream turbulence intensity were determined from these profile measurements. Fig. 5 shows the isentropic free-stream Mach number distribution along the convex test surface. The corresponding distribution of the acceleration parameter indicates a nearly zero pressure gradient flow within the relevant part of convex test section (Fig. 5). Fig. 6 shows the distributions of the boundary layer and displacement thickness versus streamwise distance, where $S/D = 0$ corresponds to the injection location. The distribution of the boundary layer thickness decreases at the entrance of the curved test section due to the accelerated free-stream flow. The ratio between the boundary layer thickness and the injection hole diameter is about $\delta/D = 0.6$, respectively $\delta_1/D = 0.09$, at the injection location. The distribution of the boundary layer thickness indicates a moderate increase within the convex test section. Because of the decelerating free-stream flow at the exit of the curved test section the distribution of the boundary layer thickness increases rapidly. The distribution of the local turbulence intensity at the edge of the boundary layer is also shown in Fig. 6. The distribution of the turbulence intensity

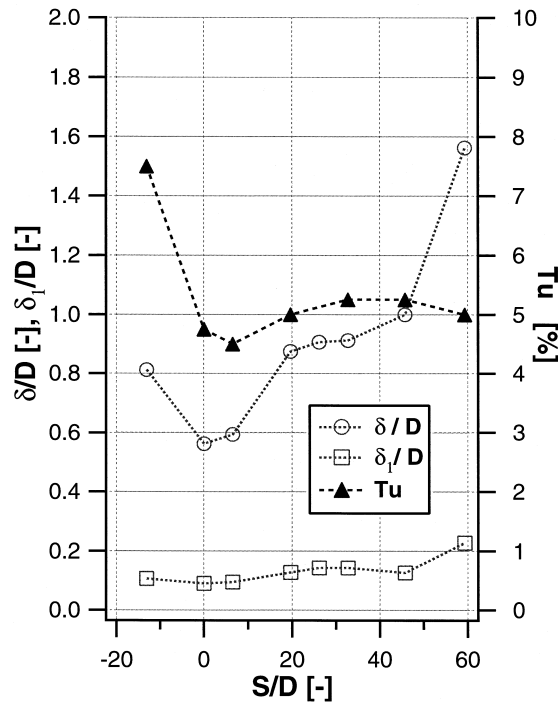


Fig. 6. Distributions of the boundary layer thickness, displacement thickness and free-stream turbulence intensity versus streamwise distance.

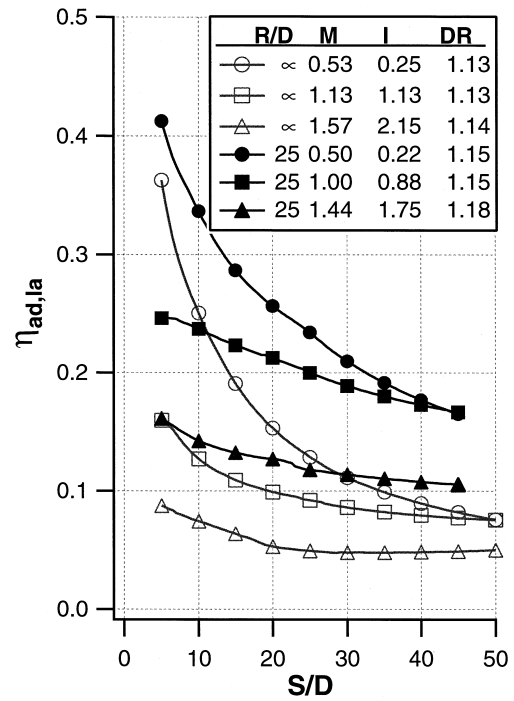


Fig. 7. Comparison of lateral averaged film cooling effectiveness values obtained on convex curved and flat surfaces with cylindrical injection.

stays nearly constant at about $Tu_\infty = 5\%$ within the relevant part of convex test section ($0 < S/D < 50$). Additional hot-wire measurements were conducted at the entrance of the convex test section ($S/D = -13$) to determine the turbulence quantities of the free-stream flow. An integral length scale of $\Lambda \approx 53$ mm and a microscale of $\lambda \approx 11$ mm were determined. These hot-wire measurements were taken 400 mm downstream of the turbulence grid.

Fig. 7 compares film cooling effectiveness values obtained on a flat [18] and convex surface for injection through cylindrical holes. The results obtained on the convex surface indicate higher film cooling effectiveness values than the corresponding data on the flat surface. The present results are, in general, agreement with results from Schwarz et al. [16]. The density ratio was varied during the experiments with injection configuration CONF 1 by using air and CO₂ as coolant fluids. A density ratio of about $DR \approx 1.15$ was attained during the experiments with air-injection and about $DR \approx 1.8$ with CO₂-injection. The results obtained with air-injection indicate generally a decreasing adiabatic film cooling effectiveness with increasing coolant mass flows (Fig. 8). The results obtained with CO₂-injection indicate an optimum adiabatic film cooling effectiveness value in a momentum ratio range of $I =$

0.2–0.5. The results from injection configuration CONF 1 obtained with air- and CO₂-injection correlated quite well with the momentum flux ratio. The film cooling performance of injection configuration CONF 2 is about 50% lower than the corresponding values from injection configuration CONF 1, which corresponds to the different hole spacing for these two injection configurations ($P/D_{CONF 1} = 3$) and ($P/D_{CONF 2} = 6$) (see Fig. 8). Fig. 9 compares lateral averaged film cooling effectiveness results obtained with cylindrical (CONFs 2 and 3) and shaped (CONFs 4 and 5) injection configurations at different coolant blowing rates $M = 0.5, 1.0, 1.5$ and 2.0 and CO₂-injection. Injection configuration CONF 3 indicates a weaker dependency on the investigated blowing rates than the corresponding results of CONF 2. Especially at higher blowing rates CONF 3 achieved higher film cooling effectiveness values due to the compound injection angle than CONF 2 with the in-line coolant injection. All injection configurations with cylindrical holes indicate an optimum film cooling effectiveness within the investigated range of coolant mass flows. The results obtained with the shaped injection configurations CONF 4 and CONF 5 indicate generally an increasing adiabatic film cooling effectiveness with increasing blowing rate. This was attributed to the reduced momentum of the coolant fluid at the hole exit due to the hole extension in lateral direction. The hole extension in lateral direction also improved the lateral spreading of the coolant fluid on the surface to be cooled. The greatest benefit of the shaped holes occurs for blowing rates $M > 1$.

As the heat transfer coefficient is dependent on the free-stream velocity and properties of the secondary fluid it is difficult to compare the heat transfer performance with experiments conducted at different free-stream boundary conditions. Therefore, the heat transfer data will be shown here as Stanton numbers. The Stanton number is defined as follows

$$St_f = \frac{h_f}{C_{p,f} \rho_f U_\infty} \tag{6}$$

where h_f and U_∞ are the local values for the heat transfer coefficient and the free-stream velocity, respectively. In the case of CO₂-injection also the values for the specific heat $C_{p,f}$ and density ρ_f are changing in streamwise direction because of the mixing between the coolant and free-stream fluids. To calculate proper values for $C_{p,f}$ and ρ_f , the results for the adiabatic film cooling effectiveness determined at the same blowing rate were used. The mixing of CO₂ and the free-stream air is then calculated by applying the analogy of heat and mass transfer [19]. With this analogy the film cooling effectiveness can be expressed in terms of a concentration ratio of coolant to free-stream for

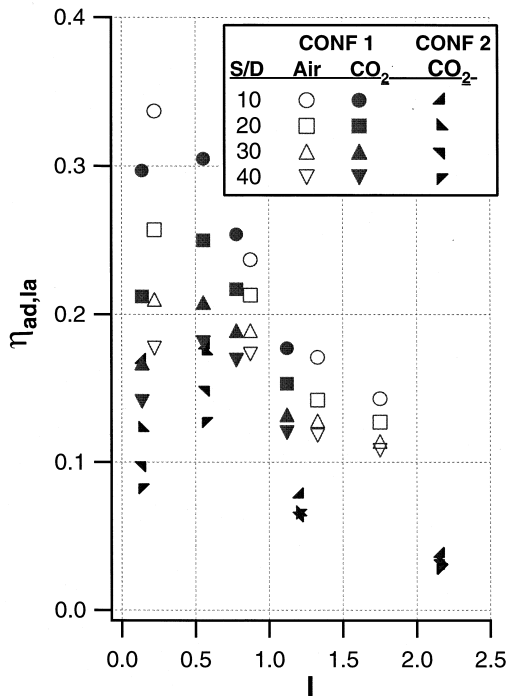


Fig. 8. Distributions of lateral averaged film cooling effectiveness values with air- and CO₂-injection versus momentum ratio.

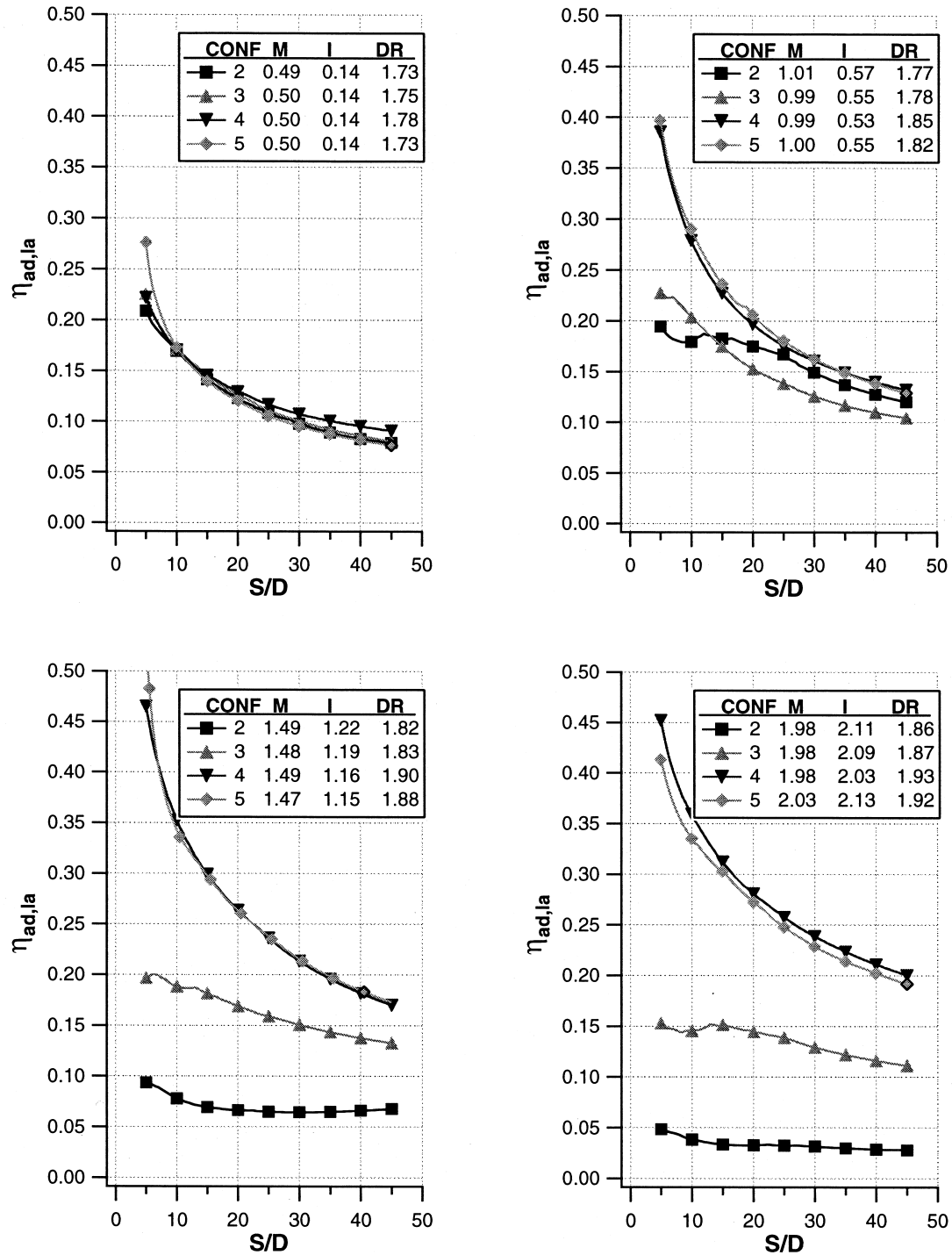


Fig. 9. Distributions of lateral averaged film cooling effectiveness values with CO₂-injection versus streamwise distance. Comparison of injection configurations.

incompressible flows

$$\eta_{ad} = \frac{T_{\infty} - T_{aw}}{T_{\infty} - T_c} = \frac{C_{\infty}^{CO_2} - C_w^{CO_2}}{C_{\infty}^{CO_2} - C_c^{CO_2}} = C_w^{CO_2} \quad (7)$$

With the CO₂ concentrations of the free-stream ($C_{\infty}^{CO_2} = 0$) and the coolant ($C_w^{CO_2} = 1$) fluid the local CO₂ concentration at the wall ($C_w^{CO_2}$) can be directly estimated from the local adiabatic film cooling effectiveness values. The local fluid properties of the air/CO₂-mixture can thus be determined to calculate the correct Stanton numbers.

Fig. 10 compares Stanton number ratios obtained on flat [20] and convex surfaces for injection through cylindrical holes. The results obtained on the convex surface indicate slightly higher increases in heat transfer in the near hole region compared to the flat plate results. The decay of heat transfer increase with down stream distance is stronger for the convex surface. Heat transfer experiments with injection configuration CONF 1 were conducted with air- and CO₂ as coolant fluids. As mentioned above, the coolant and free-stream temperatures were adjusted to be on the same level during these experiments. Therefore, a density ratio of DR = 1.0 is associated with air-injection and a density ratio of DR = 1.53 belongs to CO₂-injection.

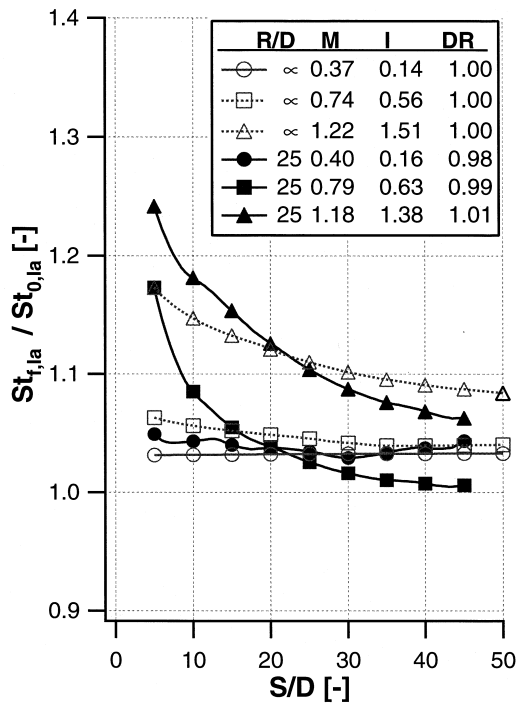


Fig. 10. Distributions of lateral averaged heat transfer ratios obtained on convex curved and flat surfaces with cylindrical injection holes.

The momentum flux ratios were matched between the measurements with air- and CO₂-injection. Fig. 11 shows lateral averaged Stanton number ratios obtained with air- and CO₂-injection for injection configuration CONF 1. The heat transfer increase due to film injection is more pronounced for air-injection. The results obtained with CO₂-injection for injection configuration CONF 2 indicate increased heat transfer ratios with increasing blowing rate as expected. The results do not indicate a reduction in heat transfer increase compared to the corresponding results from CONF 1 as expected from the larger hole spacing (CONF 1: $P/D = 3$ and CONF 2: $P/D = 6$). Fig. 12 compares lateral averaged Stanton number ratios obtained with cylindrical (CONFs 2 and 3) and shaped (CONFs 4 and 5) injection configurations at different coolant blowing rates $M = 0.5, 1.0, 1.5$ and 2.0 and CO₂-injection. The heat transfer ratios obtained with CONF 3 increase with increasing blowing rate. The heat transfer ratios obtained with CONF 3 are slightly higher than those values obtained with CONF 2. The heat transfer results obtained with the shaped injection configuration CONF 4 indicate a weaker dependency on the blowing rate than the results obtained with the cylindrical injection configurations. This is attributed to the reduction in coolant exit momentum due to the hole extension. The reduced coolant exit momentum caused

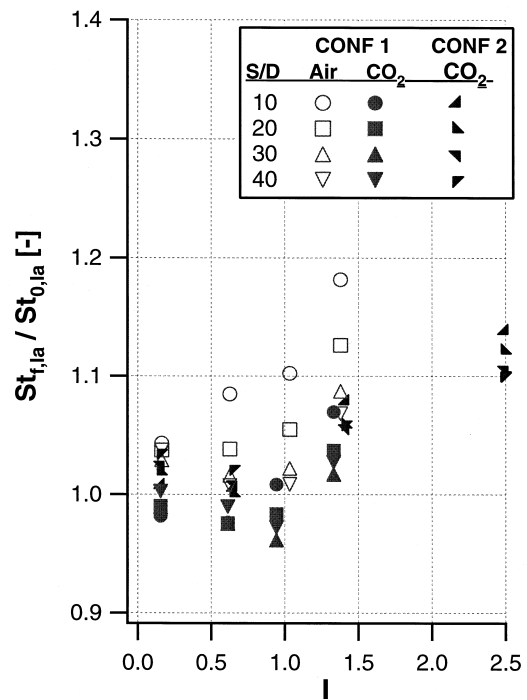


Fig. 11. Distributions of lateral averaged Stanton number ratios with air and CO₂-injection versus momentum ratio.

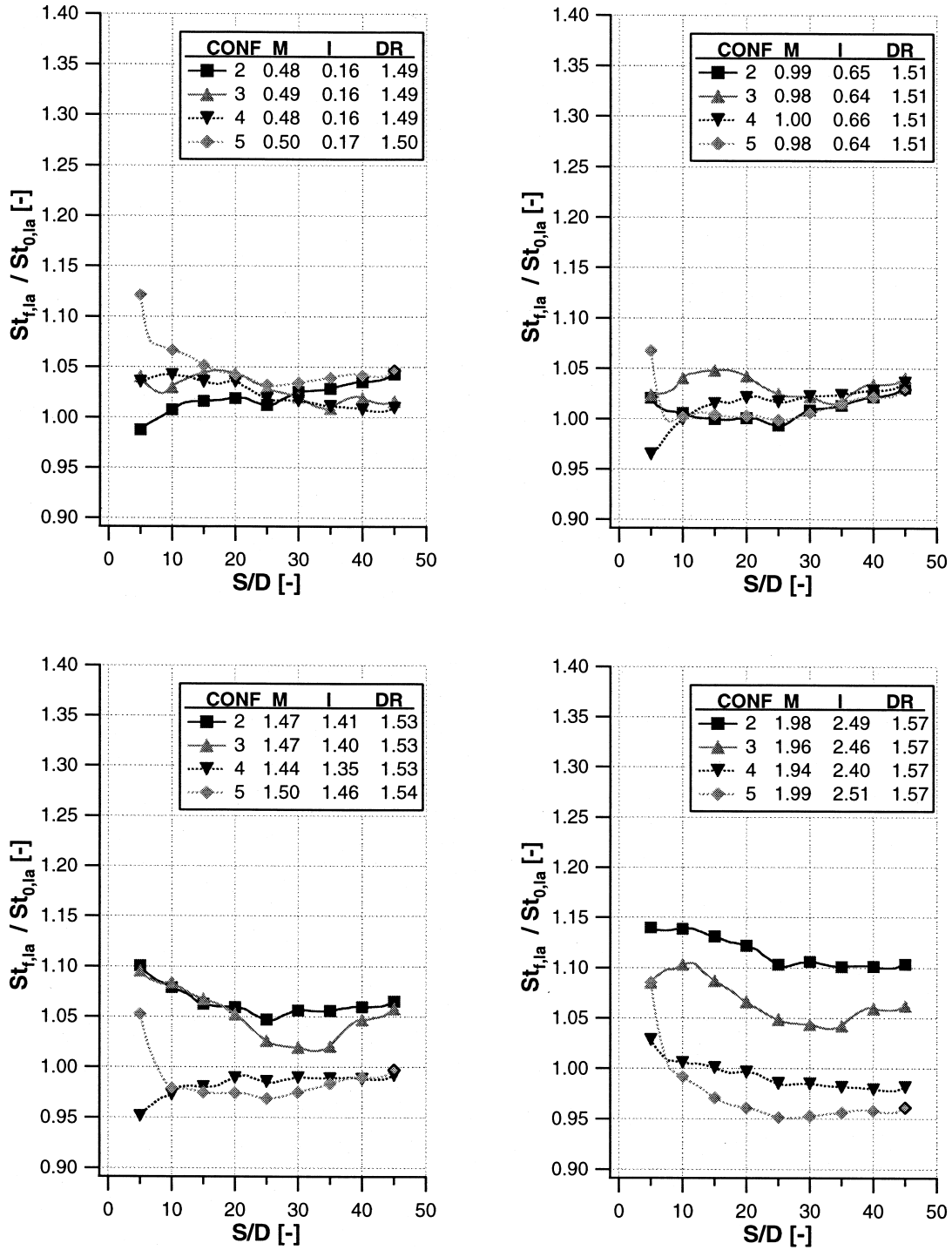


Fig. 12. Distributions of lateral averaged heat transfer ratios with CO₂-injection versus streamwise distance. Comparison of injection configurations.

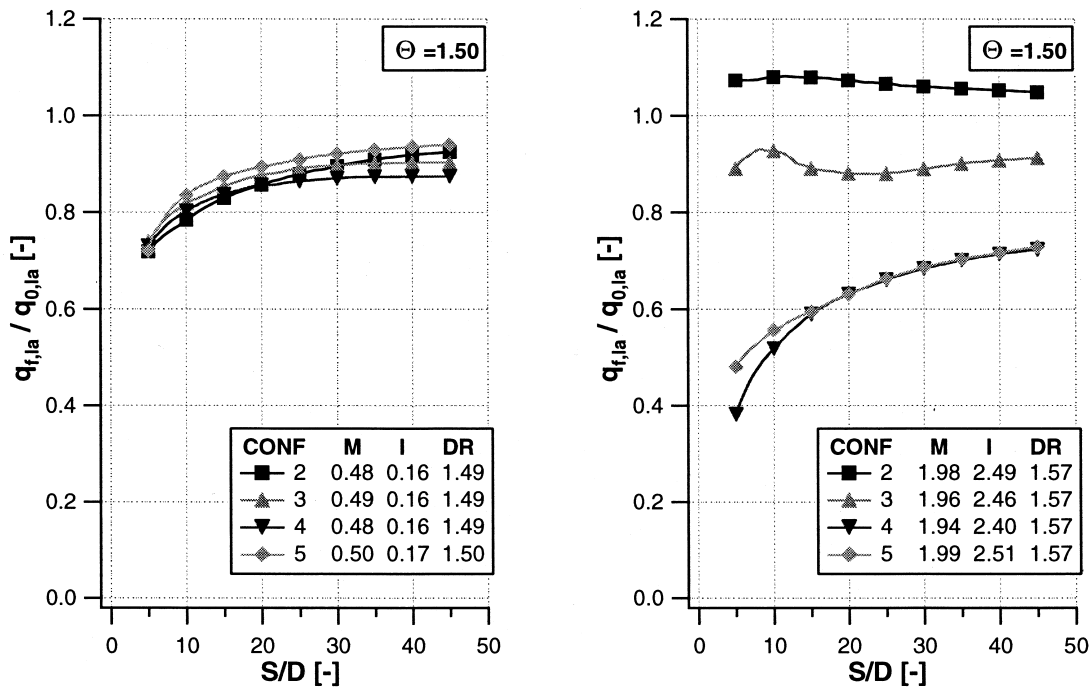


Fig. 13. Distributions of heat flux ratios with CO₂-injection versus streamwise distance for all investigated injection configurations and blowing rates $M = 0.5$ and 2.0 .

less flow disturbance of the free-stream flow and lead, therefore, to less heat transfer increase even at high blowing rates. The heat transfer results obtained with the shaped injection configuration CONF 5 indicate even less dependency on the blowing rate as the results obtained with CONF 4. There is a quite strong increase in heat transfer due to coolant injection close to the injection location. This is caused by local flow separations within or just downstream of these laid back shaped injection holes. However, this increased heat transfer vanished rapidly with downstream distance. The results obtained further downstream ($S/D > 25$) indicate the lowest heat transfer ratios from all injection configurations investigated. The results obtained with the cylindrical injection configurations indicate the highest heat transfer ratios at high blowing rates. As already mentioned during the adiabatic film cooling results the highest benefit of the shaped injection configurations occurred at high blowing rates.

The previously presented results provide separate information on the film cooling performance in terms of the adiabatic film cooling effectiveness values and the heat transfer coefficients. In general, an injection of a coolant on the surface causes a lower wall temperature but increases the heat transfer coefficient. To indicate the quality of a film cooling configuration, these two

pieces of information have to be considered at the same time. The main goal in the film cooling design process is to find an optimally way to keep the surface temperature at a certain level T_w . The total performance of one film cooling configuration can then be expressed by the ratio of the heat fluxes with film cooling applied and the heat flux without film cooling.

The heat flux without film cooling can be determined from Eq. (3)

$$\dot{q}_0 = h_0(T_{r,\infty} - T_w). \tag{8}$$

With film cooling applied the heat flux can be determined from Eq. (5)

$$\dot{q}_f = h_f(T_{aw} - T_w). \tag{9}$$

The ratio of these two heat fluxes can thus be expressed as

$$\frac{\dot{q}_f}{\dot{q}_0} = \frac{h_f (T_{aw} - T_w)}{h_0 (T_{r,\infty} - T_w)}. \tag{10}$$

With the definition of the adiabatic film cooling effectiveness and a dimensionless wall temperature Θ this ratio can be expressed for a defined wall temperature as

$$\frac{\dot{q}_f}{\dot{q}_0} = \frac{h_f}{h_0} (1 - \eta_{ad} \Theta) \quad (11)$$

where Θ is defined as

$$\Theta = \frac{T_{r, \infty} - T_c}{T_{r, \infty} - T_w} \quad (12)$$

Θ describes the boundary conditions of the cooling process. By setting a reasonable value for Θ , with the determined values for the adiabatic film cooling effectiveness and the heat transfer coefficient, the heat flux ratio \dot{q}_f/\dot{q}_0 can easily be calculated. As the ratio \dot{q}_f/\dot{q}_0 is different for each injection configuration and varies with the blowing rate it can be seen as an indicator of the film cooling quality at a certain blowing rate. Heat flux ratios below 1 indicate a reduction of the heat flux into the surface that needs to be cooled. Heat flux ratios above 1 indicate that the film cooling process increases the heat flux into the surface compared to the case without film cooling.

Fig. 13 compares lateral averaged heat flux ratios determined for cylindrical (CONFs 2 and 3) and shaped (CONFs 4 and 5) injection configurations at different coolant blowing rates $M = 0.5$ and 2.0 for CO_2 -injection. The dimensionless wall temperature was set to a value of $\Theta = 1.5$. All injection configuration show similar distributions at a low blowing rate of $M = 0.5$. Close to the injection holes ($S/D = 5$) a heat flux reduction of about 50% is achieved. At a downstream distance of $S/D = 50$ still a heat flux reduction of about 10% is maintained. For high blowing rate of $M = 2.0$ only the shaped injection configurations provide a good film cooling performance of 40–50% at $S/D = 5$ and 30% at $S/D = 50$. Injection configuration CONF 4 indicates a slightly better film cooling performance in the near hole region compared to CONF 5. The compound angle injection configuration CONF 3 shows a heat flux reduction of 10% for the investigated range downstream of coolant injection. Injection configuration CONF 2 indicates a heat flux penalty at the high blowing rate. The heat flux into the surface is additionally increased by 5–8% due to film injection.

5. Conclusions

An overview on the available literature concerning film cooling investigations on curved walls indicate that curvature has a significant influence on the film cooling performance. However, there is not sufficient data available to deduce physical models or design correlations describing the film cooling behaviour on air-foil pressure and suction sides. The design features of the convex curved test section, which will be the basis for further subsequent test section designs, was

described. The test section has a ratio of surface curvature radius to film hole diameter of $R/D = 25$. The free-stream follows a 150° -bend in the test section, with secondary fluid (CO_2 or air) or air injection at a bend angle of $\gamma_{inj} = 30^\circ$. Five different injection configurations were investigated during this film cooling test program. The multiple narrow-banded thermo-chromic liquid crystal wall surface temperature measurement technique was used for the measurement of the adiabatic film cooling effectiveness and heat transfer coefficient.

The current experiments were conducted with a constant free-stream Mach number of $Ma_\infty = 0.4$ with an increased free-stream turbulence intensity of $Tu_\infty = 5\%$. Aerodynamic measurements were conducted to determine the flow field of the convex test section. Distributions of the boundary layer thickness and free-stream turbulence intensities were determined by hot-wire traverses. The cylindrical hole injection configurations, CONF 1 and CONF 2, indicate a significant decrease in film cooling effectiveness and an increase in heat transfer at moderate and high blowing rates. This was attributed to separation of the coolant fluid. The third injection configuration with cylindrical holes, CONF 3, indicated better film cooling effectiveness values due to the compound angle injection. However, the heat transfer increase was slightly higher compared with results obtained with injection configurations CONF 2. The shaped hole injection configurations, CONF 4 and CONF 5, achieved the best film cooling performance compared with the other injection configurations. The second shaped injection configuration with an additional laid back angle, CONF 5, indicated slightly less film cooling performance close to the injection location than CONF 4. This was attributed to local flow separations within or just downstream of these laid back shaped holes.

Acknowledgements

This work is carried out within the Brite EuRam project 'Turbine Aero-Thermal External Flows' (BE97-4440). The authors wish to acknowledge the fruitful collaboration with the partners within the Brite EuRam project and their permission to publish this paper. Additionally the authors would like to thank ABB Alstom Power and ABB Alstom Technology for permission to publish this paper. The first author wish to acknowledge the help of T. Scheller and R. Digele for conducting the film cooling experiments described in this paper.

References

- [1] J. Nicolas, A. Le Meur, Curvature Effects on a Turbine Blade Cooling Film, ASME, New York, 1974 (74-GT-156).
- [2] C.O. Folyan, J.H. Whitelaw, The Effectiveness of Two-Dimensional Film-Cooling over Curved Surfaces., 1976 ASME, New York (76-HT-31).
- [3] R.E. Mayle, F.C. Kopper, M.F. Blair, D.A. Bailey, Effect of streamline curvature on film cooling, J. Engineering for Power 99 (1977) 77–82.
- [4] S. Ito, R.J. Goldstein, E.R.G. Eckert, Film cooling of a gas turbine blade, J. Engineering for Power 100 (1978) 476–481.
- [5] W. Rodi, W. Haas, B. Schönung, Untersuchung des Grenzschichtverhaltens an Turbinenschaukeln unter Berücksichtigung von Filmkühlung und von lokalen Ablöseblasen, FVV Vorhaben Nr. 310, 1983-1986.
- [6] K. Takeishi, S. Aoki, T. Sato, K. Tsukagoshi, Film Cooling on a Gas Turbine Rotor Blade, ASME, New York, 1991 (91-GT-279).
- [7] S. Ou, J.C. Han, Unsteady wake effects on film effectiveness and heat transfer coefficient from a turbine blade with one row of air and CO₂ film injection, J. Heat Transfer 116 (1994) 921–928.
- [8] R.D. Lander, R.W. Fish, M. Suo, External heat transfer distribution on film cooled turbine vanes, J. Aircraft 9 (1972) 707–714.
- [9] R.J. Goldstein, Y. Kornblum, E.R.G. Eckert, Film cooling effectiveness on a turbine blade, Israel J. of Technology 20 (1982) 193–200.
- [10] K. Takeishi, M. Matsuura, S. Aoki, T. Sato, An experimental study of heat transfer and film cooling on low aspect ratio turbine nozzles, J. Turbomachinery 112 (1990) 488–496.
- [11] F.A. Buck, C. Prakash, Design and Evaluation of a Single Passage Test Model to Obtain Turbine Airfoil Film Cooling Effectiveness Data, ASME, New York, 1995 (95-GT-19).
- [12] S.-Y. Ko, J.-Z. Xu, Y.-Q. Yao, F.K. Tsou, Film cooling effectiveness and turbulence distribution of discrete holes on a convex surface, J. Heat Mass Transfer 27 (1984) 1551–1557.
- [13] H. Kruse, Effects of hole geometry, wall curvature and pressure gradient on film cooling downstream of a single row, in: AGARD Conference Proceedings, vol. 309, 1985, pp. 8.1–8.13.
- [14] T.S. Lee, J.S. Lee, S.W. Lee, Experimental study on the effect on concave and convex curvature on film cooling effectiveness, in: Proceedings of the 9th Int. Heat Transfer Conference Jerusalem Israel, vol. 6, 1990, pp. 341–346.
- [15] S.G. Schwarz, R.J. Goldstein, The Two-Dimensional Behaviour of Film Cooling Jets on Concave Surfaces, ASME, New York, 1988 (88-GT-161).
- [16] S.G. Schwarz, R.J. Goldstein, E.R.G. Eckert, The influence of curvature on film cooling performance, J. Turbomachinery 113 (1991) 472–478.
- [17] D.M. Kercher, A film-cooling CFD bibliography: 1971–1996, Int. J. Rotating Machines 4 (1998) 61–72.
- [18] E. Lutum, B.V. Johnson, Influence of the hole length-to-diameter ratio on film cooling with cylindrical holes, J. Turbomachinery 121 (1999) 209–216.
- [19] J.N. Shadid, E.R.G. Eckert, The mass transfer analogy to heat transfer fluids with temperature-dependent properties, J. Turbomachinery 113 (1991) 27–33.
- [20] B. Weigand, M.E. Crawford, E. Lutum, A Computational and experimental investigation of the effect of surface roughness on film cooling, in: Proceedings of the 7th International Symposium on Transport Phenomena and Dynamics of Rotating Machinery, ISROMAC-7, Honolulu, Hawaii, USA, Springer, Berlin, 1998, pp. 1683–1692.